Article

A High Power Factor LED Driver with Intrinsic Current Balancing Capability

Hung-Liang Cheng *[ID] **and Yi-Chan Hung**

Department of Electrical Engineering, I-Shou University, Dashu District, Kaohsiung City 84001, Taiwan; antonio19991031@gmail.com
* Correspondence: hlcheng@isu.edu.tw; Tel.: +886-7-657-7711 (ext. 6634)

Abstract: The research proposed a novel LED driver with the functions of power-factor correction (PFC) and current balancing. A flyback converter and a Class-D series resonant converter were integrated by sharing an active switch to form a single-stage circuit topology. The flyback converter played the role of a PFC circuit. The component parameters were designed to make the flyback converter to operate at discontinuous-conduction mode (DCM). In this way, the input line current can be sinusoidal, resulting in near unity power factor and low total harmonic distortion in current (THDi). The resonant converter was connected in series with a differential-mode transformer with a turns ratio of 1 to drive four LED strings. The current of the four LED strings will be automatically and evenly balanced by using the 1:1 transformer. This article analyzed the different modes of operation in detail, derived the mathematical equations and designed the parameters of the circuit components. Finally, a 72-W prototype LED driver was implemented and tested. A satisfactory performance has verified the feasibility of the proposed LED driver.

Keywords: Class-D resonant converter; current balancing; flyback converter; light-emitting diode (LED); power-factor correction; single-stage

1. Introduction

Light-emitting diodes (LED) have a much longer lifespan than traditional light sources, due to continuous innovation and advancement in manufacturing techniques and materials. Generally, the service life of LEDs can reach about 100,000 h, whereas fluorescent lamps and incandescent bulbs typically last only a few thousand hours. In addition, LED has many benefits, including compact size, high energy efficiency, good color rendering, fast response speed, and so on. These advantages mean that LEDs are widely used in many light applications [1–3]. Nowadays, the power level of a high-brightness LED is approximately hundreds of milliwatts to several watts. For large luminous lighting systems, a large number of LEDs are required to meet high power requirements. These LEDs are connected in combinations of series and/or parallel connections [4,5].

Even for the same type of LED, the voltage–current characteristic curve of each LED will inevitably have slight differences. Moreover, connecting multiple LEDs in series will amplify the difference between each LED string, resulting in unbalanced LED current in each string. What is more serious is that LED has a negative temperature coefficient characteristic, that is, its forward voltage decreases with the increase of temperature. This negative temperature coefficient characteristic will aggravate the current imbalance between the strings and even cause the LED to burn out due to thermal runaway. Therefore, the study of current balancing techniques for parallel-connected LEDs is an important topic for LED lighting apparatuses. This helps to extend the life of the LEDs and ensures that they all operate at their maximum efficiency. For lower power lighting equipment, current-mirror technology is usually used to achieve current balancing [6–8]. Current-mirror technology uses transistors in series with each LED string. These transistors are

controlled to have the same current, i.e., the same current in the LED strings. Since these transistors are not operated as switches and their conducting voltages are high, resulting in large conduction losses.

The active current-balancing techniques use logic circuits to regulate the current of each string of LEDs [9–12]. This method requires a more complex circuit and is more expensive because all LED strings require separate current control loops and drive circuits. Passive current-balancing techniques use passive components such as diodes, inductors, capacitors or transformers [13–18]. Compared to active techniques, passive techniques are simpler because no additional active switches and complex control circuitry are required. Among them, some techniques use multiple transformers with primary windings connected in series so that the secondary windings can have the same current [13,14]. Other methods place each LED string in series with a capacitor and/or inductor with high impedance. Using high-impedance inductors or capacitors can effectively alleviate the influence of current imbalance caused by differences in LED equivalent resistance [15,16]. Nevertheless, these approaches require the use of bulky transformers, inductors, or capacitors. References [17,18] used the ampere-second balance principle of capacitance to automatically balance the current between LED strings. The disadvantage is that, when expanding the number of LED strings, it is necessary to add resonant inductors and capacitors, resulting in a large increase in the number of components. A series resonant converter has the advantage of low switching losses due to zero-voltage switching on (ZVS) when it is designed to operate with an inductive load. In addition, its resonant capacitor can block the DC component of the input voltage so that the resonant current flowing through it is a pure AC component. In other words, the forward average value of the resonant current is the same as the reverse average value. When the load is two anti-parallel LED strings, the currents flowing through the LED strings are automatically equal without adding any components for current balancing [19,20].

Another research topic related to LED drivers is PFC; the power factor and THDi of lighting equipment must comply with standards such as IEC 61000-3-2 Class D and IEEE 519. Therefore, LED drivers must use an additional ac/dc, which serves as a power-factor correction (PFC) circuit to satisfy these standards. It results in a two-stage circuit topology. The first stage is a PFC circuit to shape the input current into a sine wave and the second stage is a dc/dc converter to regulate the LED voltage. Although performing well, the two-stage approach requires more circuit components. Aiming to reduce the number of components and to improve energy conversion efficiency, many single-stage LED drivers which integrate the PFC circuit and the dc/dc converter have been proposed [21–25]. In references [21,22], the PFC circuits are boost converters, which are operated at either boundary-conduction mode (BCM) or discontinuous-current mode (DCM). Operating the boost converter at BCM or DCM can achieve a high power factor with easier control. However, when a boost converter operates at BCM or DCM, the dc-bus voltage should be at least twice the peak of the ac input to achieve a nearly unity power factor. In contrast, buck-boost or flyback converters are also commonly used as PFC circuits. However, they have no such limitation on the dc-link voltage. A high power factor can be achieved by operating them at a fixed switching frequency and a fixed duty cycle over the line frequency cycle [23–25]. In reference [23,24], a buck-boost converter was used as the PFC circuit, while in reference [25] a flyback converter was used. Typically, the LED voltage is much lower than the magnitude of the input voltage. The flyback converter uses a coupled inductor as an energy storage component and the winding turns ratio can be selected according to the output voltage specification. When the primary-to-secondary turns ratio is high, the voltage rating of the dc/dc converter can be effectively reduced.

In this paper, a new single-stage LED driver derived by integrating a flyback-typed PFC circuit and a Class-D series resonant converter was proposed. One of the two active switches of the resonant converter was shared with the flyback converter. The flyback converter served as the PFC circuit while the Class-D series resonant converter served as the dc/dc converter. A differential-mode transformer was added to the resonant converter [26].

With this 1:1 turns ratio transformer, the automatic current balancing capability can be extended to four LED strings without resorting to any complex control circuitry. This paper is organized as follows. Section 2 describes the circuit topology of the LED driver and the circuit operation in different operating modes. Detailed circuit analyses, an illustrative prototype, and the experimental results of LED driver are provided in Sections 3 and 4, respectively. Finally, some conclusions are given in Section 5.

2. Analysis of the Proposed LED Driver Circuit

By integrating a flyback converter and a Class-D series resonant converter, the novel single-stage LED driver was proposed, as shown in Figure 1. The load was composed of four strings of LEDs. There were two MOSFETs, S_1 and S_2, with intrinsic body diodes D_{S1} and D_{S2}, respectively. The flyback converter consists of a coupled inductor T_1, a MOSFET S_2, a diode D_1, and a dc-link capacitor C_{dc}. It is operated at a discontinuous-conduction mode (DCM). In this way, in each high-frequency cycle, the primary current of T_1 is triangular-shaped, and its peak value in each high-frequency cycle forms a sinusoidal envelope. A low-pass filter (L_f and C_f) can remove the high frequency components of the primary current and the input line source only needs to provide the average value. The series resonant converter consists of S_1, S_2, a resonant tank (L_r and C_r), a diode D_3, and a differential-mode transformer T_2. The turn ratio of T_2 is equal to one. Therefore, the primary and secondary currents of T_2 are equal.
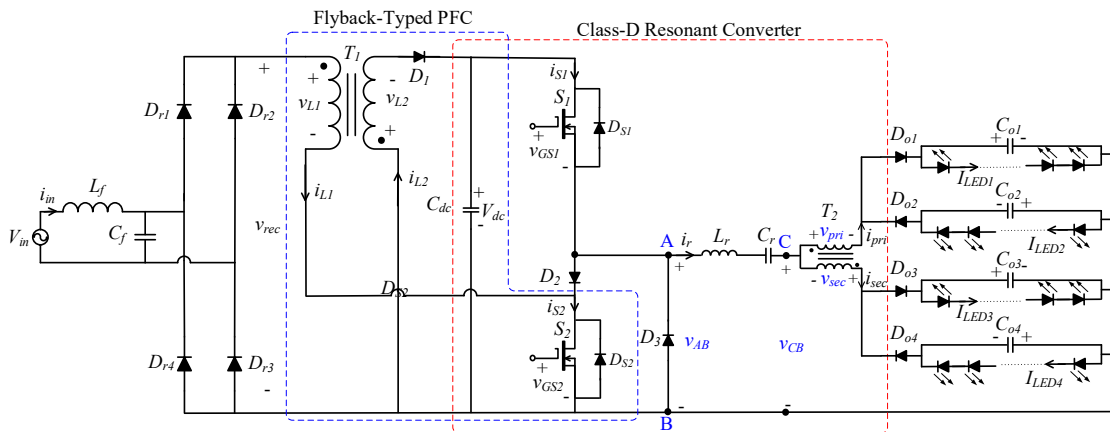
Figure 1. Proposed single-stage LED driver.

The input voltage is sinusoidal.

$$v_{in}(t) = V_m \sin\left(2\pi f_L t\right), \tag{1}$$

where f_L and V_m are the frequency and amplitude of the input voltage, respectively.

S_1 and S_2 are alternatively turned on and off by two high-frequency gate voltages, v_{GS1} and v_{GS2}. They are a pair of symmetrical and complementary and square wave voltages. There is a short deadtime between them to avoid simultaneous conduction of S_1 and S_2.

To simplify the circuit analysis, the following assumptions were made:

1. All components are considered ideal;
2. The leakage inductance of T_1 and T_2 is negligible in comparison to the magnetizing inductance;
3. The switching frequency (f_s) of S_1 and S_2 is far higher than f_L, thus, V_{in} is considered constant in a high-frequency period;
4. The capacitances C_{dc} and C_{o1}–C_{o4} are large enough so that the voltages across them (V_{dc}, V_{o1}–V_{o4}) are constant at steady-state operation;
5. The current of each LED string is equal. ($I_{LED1} = I_{LED2} = I_{LED3} = I_{LED4} = I_{LED}$).

Based on these assumptions, there will be six modes of operation in a high frequency cycle at a steady state. Figure 2 shows the current loops for each mode, where v_{rec} is the rectified line voltage and R_1–R_4 represent the equivalent resistance of these four LED strings. Figure 3 illustrates the key waveforms of the proposed circuit in high-switching cycles. The circuit operation of each mode was analyzed as follows.
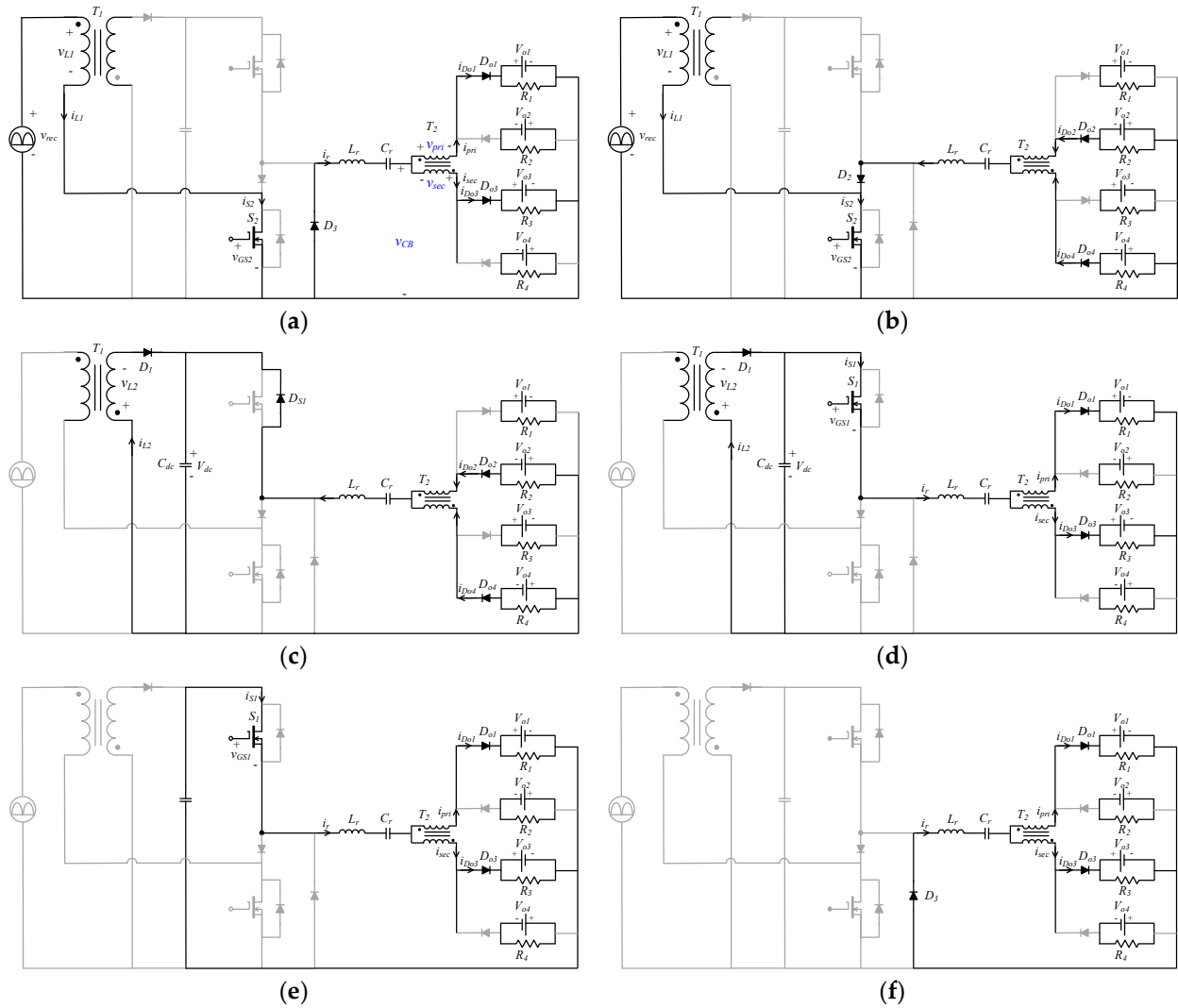
Figure 2. Equivalent circuits (**a**) Operation Mode I; (**b**) Operation Mode II; (**c**) Operation Mode III; (**d**) Operation Mode IV; (**e**) Operation Mode V; (**f**) Operation Mode VI.

2.1. Mode I ($t_0 < t < t_1$)

Mode I begins at time t_0 as soon as the gate signal v_{GS2} goes from a low to a high level to turn on S_2. Figure 2a shows the equivalent circuit of Mode I. The primary inductance voltage of T_1 is equal to the rectified input voltage. Owing to DCM operation, the primary current i_{L1} rises from zero linearly.

$$v_{L1}(t) = V_m|\sin(2\pi f_L t)|, \tag{2}$$

$$i_{L1}(t) = \frac{V_m|\sin(2\pi f_L t)|}{L_1}(t - t_0), \tag{3}$$

where L_1 is the primary inductance of T_1. As shown in the equivalent circuit, the input voltage of the series resonant converter is zero volts.
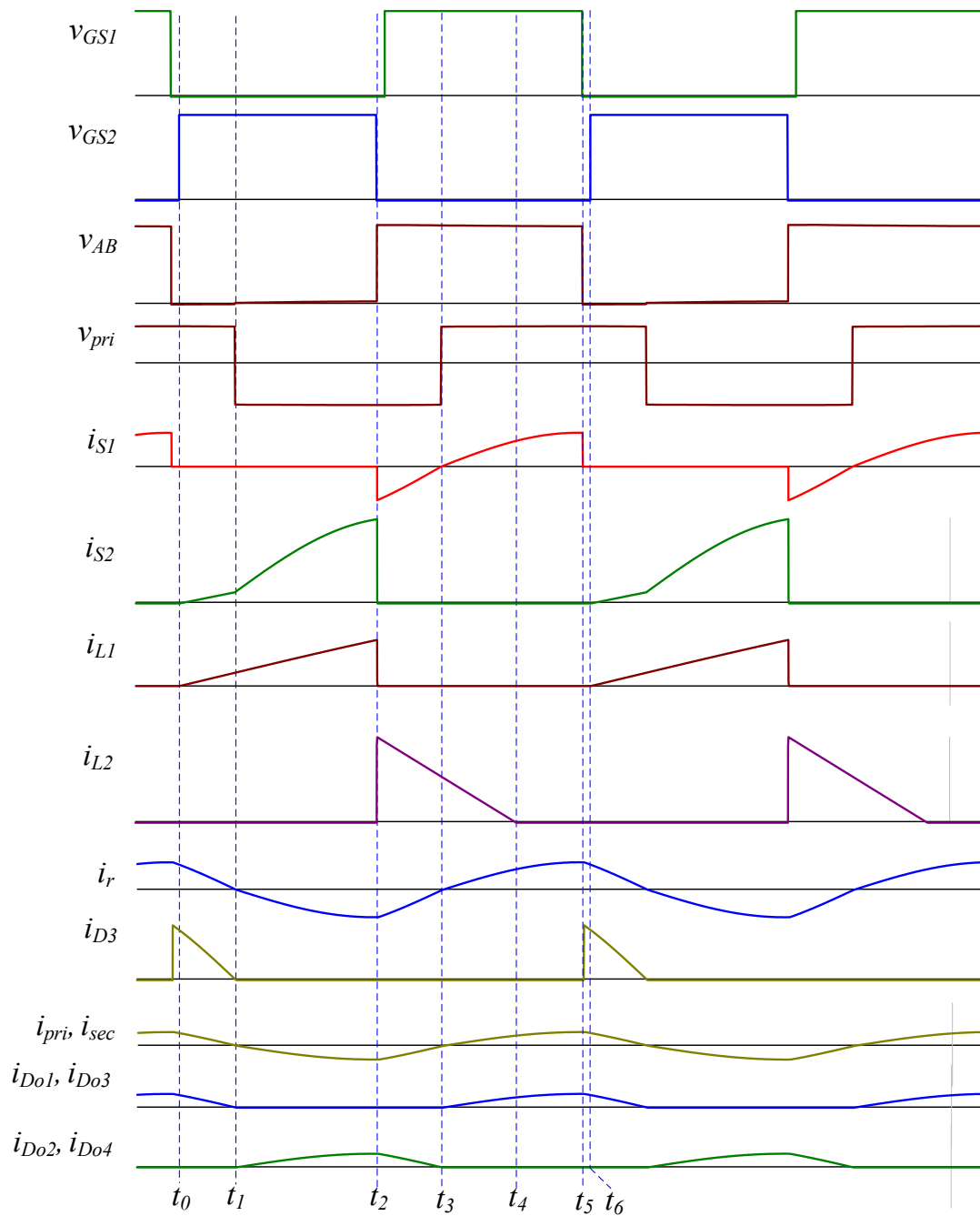
Figure 3. Schematic waveforms of voltage and current in the LED driver.

$$v_{AB}(t) = 0. \tag{4}$$

The resonant current i_r is positive and flows through both windings of T_2, D_{o1}, D_{o3}, and D_3. The turn ratio of T_2 is equal to 1, so the winding currents are equal to half of i_r.

$$i_{Do1}(t) = i_{pri}(t) = \frac{i_r(t)}{2}, \tag{5}$$

$$i_{Do3}(t) = i_{sec}(t) = \frac{i_r(t)}{2}. \tag{6}$$

Applying Kirchhoff's voltage law to the resonant current loop yields the following equations.

$$v_{CB}(t) = v_{pri}(t) + V_{o1} = -v_{sec}(t) + V_{o3}. \tag{7}$$

With a turn ration of 1, the primary winding voltage v_{pri} and the secondary winding voltage v_{sec} are equal. From Equation (7), v_{CB}, v_{pri}, and v_{sec}, can be obtained.

$$v_{pri}(t) = v_{sec}(t) = \frac{V_{o3} - V_{o1}}{2}, \tag{8}$$

$$v_{CB}(t) = \frac{V_{o1} + V_{o3}}{2}. \tag{9}$$

When i_r resonates to zero and changes its polarity, the circuit enters mode II.

2.2. Mode II ($t_1 < t < t_2$)

S_2 remains on, and v_{L1} and i_{L1} equations are the same as Equations (2) and (3). The current i_{L1} increases continuously and linearly. In this mode, i_r becomes negative and flows through both windings of T_2, D_{o2}, D_{o4}, D_2, and S_2.

$$i_{Do2}(t) = -i_{pri}(t) = \frac{-i_r(t)}{2}, \tag{10}$$

$$i_{Do4}(t) = -i_{sec}(t) = \frac{-i_r(t)}{2}. \tag{11}$$

Applying Kirchhoff's voltage law to the resonant current loop yields

$$v_{CB}(t) = v_{pri}(t) - V_{o2} = -v_{sec}(t) - V_{o4}. \tag{12}$$

From Equation (12), v_{CB}, v_{pri} and v_{sec}, can be obtained.

$$v_{pri}(t) = v_{sec}(t) = \frac{-V_{o4} + V_{o2}}{2}, \tag{13}$$

$$v_{CB}(t) = \frac{-(V_{o2} + V_{o4})}{2}. \tag{14}$$

When v_{GS2} becomes zero volts, S_2 is switched off and the circuit goes to Mode III.

2.3. Mode III ($t_2 < t < t_3$)

Prior to this mode, both currents i_{L1} and i_r flow through S_2, and i_{L1} reaches a peak value expressed as

$$i_{L1,peak}(t) = \frac{V_m|\sin(2\pi f_L t)|}{L_1}(t_2 - t_0) = \frac{V_m|\sin(2\pi f_L t)|}{L_1}DT_s, \tag{15}$$

where T_s and D represent the switching cycle and duty ratio of S_2. An induced current in the secondary winding of T_1 will be generated to make the magnetic flux through the core of T_1 be consistent. The induced current i_{L2} flows through D_1 to charge the dc-link capacitor C_{dc}. The voltage across L_2 is equal to $-V_{dc}$, so i_{L2} declines.

$$i_{L2}(t) = ni_{L1, peak}(t) - \frac{V_{dc}}{L_2}(t - t_2), \tag{16}$$

where L_2 represents the secondary inductance of T_1 and n denotes the ratio of the number of turns of the primary winding to that of the secondary winding ($n = N_1/N_2$).

At the beginning of this mode, i_r diverts from S_2 to flow through the intrinsic diode D_{S1}. As shown in Figure 3, i_r is in the negative half cycle of its sinusoidal waveform and gradually rises. After a short deadtime after S_2 is turned off, v_{GS1} changes from zero volts to a high-level voltage. Since i_r is still negative, it will keep flowing through D_{S1}. The input voltage of the resonant converter is equal to the dc-link voltage. The voltage and current equations for i_{Do2}, i_{Do4}, v_{pri}, v_{sec}, and v_{CB} are the same as Equations (10)–(14). When i_r rises to pass the zero-crossing point, it changes polarity and starts to flow through S_1, and the circuit enters operation Mode IV.

2.4. Mode IV ($t_3 < t < t_4$)

Current i_r is positive and flows through both windings of T_2, D_{o1}, D_{o3}, and S_1. The voltage and current equations for i_{Do1}, i_{Do3}, v_{pri}, v_{sec}, and v_{CB} are the same as Equations (5)–(9). For the flyback PFC circuit, i_{L2} keeps declining. When i_{L2} declines to zero, the circuit enters Mode V.

2.5. Mode V ($t_4 < t < t_5$)

In this mode, there is no current in the flyback converter. Only the dc-link capacitor continuously supplies current to the load resonant circuit. S_1 is turned off as soon as v_{GS1} becomes zero volts and the circuit enters Mode VI.

2.6. Mode VI ($t_5 < t < t_6$)

Mode VI has the same resonant current loop as Mode I; therefore, the voltage and current equations for i_{Do1}, i_{Do3}, v_{pri}, v_{sec}, and v_{CB} are the same as in Equations (5)–(9). When v_{GS2} changes from zero volts to a high level, S_2 is turned on and the circuit operation goes into Mode I of the next high frequency cycle.

3. Mathematical Equations for Parameters Design

3.1. Flyback-Typed Power-Factor Correction Circuit

Based on analysis of the operation modes, i_{L1} rises linearly from zero at the beginning of Mode I and reaches a peak value at the end of Mode II. From (3), the peak value of i_{L1} is equal to

$$i_{L1,\,peak}(t) = \frac{DT_s V_m \sin(2\pi f_L t)}{L_1} = \frac{DV_m \sin(2\pi f_L t)}{L_1 f_s}, \tag{17}$$

where D represents the duty ratio of S_2. Figure 4 shows the conceptual waveform of T_1 primary current and the input current. The cutoff frequency of L_f and C_f will be designed to be less than one-eighth of f_s so that most of the high-frequency components of i_{L1} can be removed and the line input voltage only provides the average of i_{L1} over one high frequency cycle.

$$i_{in}(t) = \overline{i_{L1}(t)} = \frac{1}{T_S} \int_0^{T_s} i_{L1}(t) \cdot dt = \frac{D^2 V_m}{2L_1 f_s} \sin(2\pi f_L t). \tag{18}$$

It can be seen from Equation (18) that the line current is not only sinusoidal but also in phase with the input voltage. Therefore, high power factor and low THDi ca be obtained. The input power can be derived and expressed as

$$P_{in} = \frac{1}{\pi} \int_0^\pi V_m \sin(2\pi f_L t) \cdot i_{in}(t) d(2\pi f_L t) = \frac{D^2 V_m^2}{4L_1 f_s}. \tag{19}$$
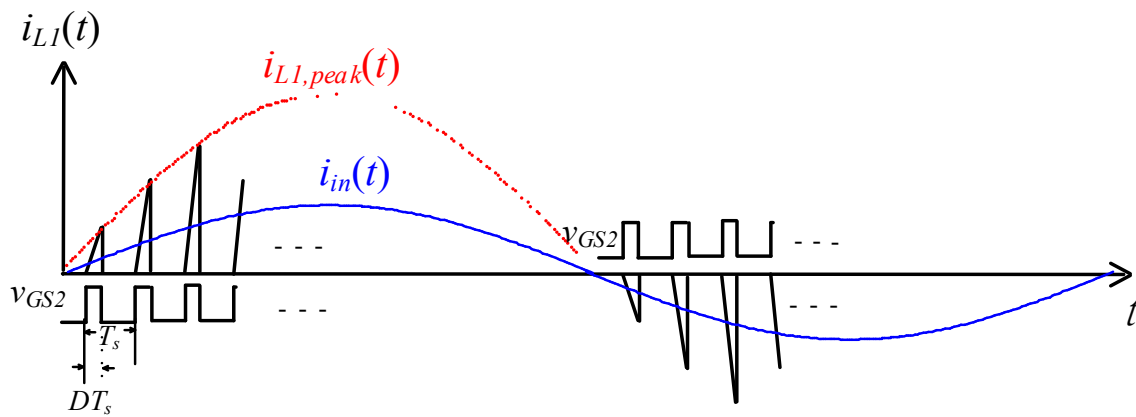
Figure 4. Conceptual waveform of T_1 primary current and input current.

The *LED* power can be expressed as

$$P_{LED} = \frac{\eta D^2 V_m^2}{4 L_1 f_s},$$ (20)

where η represents the energy-conversion efficiency. Equation (20) indicates that the output power can be controlled by regulating either the switching frequency or the duty ratio.

To ensure DCM operation, the drop time of the T_1 secondary current from peak to zero must be less than $(1-D)T_s$.

$$T_{off}(t) = \frac{V_m |\sin(2\pi f_L t)|}{n V_{dc}} D T_s < (1-D)T_s.$$ (21)

From Equation (21), when V_{dc} is high enough, it is guaranteed that the flyback converter can operate at DCM during the entire period of the input voltage.

$$V_{dc} > \frac{D V_m}{n(1-D)},$$ (22)

3.2. Class-D Series Resonant Converter

The equivalent circuit of the series resonant converter is shown in Figure 5a. According to the analysis of operation modes, the input voltage of the resonant converter is expressed as

$$v_{AB}(t) = \begin{cases} V_{dc}, & \text{for } 0 < \omega t \leq \pi \\ 0, & \text{for } \pi < \omega t \leq 2\pi \end{cases}.$$ (23)

This voltage can be expanded into Fourier series,

$$v_{AB}(t) = \frac{V_{dc}}{2} + \sum_{n=1,\,3,\,5,\,...} \frac{2 V_{dc}}{n\pi} \sin(n\omega t).$$ (24)

The root-mean-square value of the fundamental voltage of v_{AB} is given by

$$V_{1,\,rms} = \frac{\sqrt{2} V_{dc}}{\pi}.$$ (25)
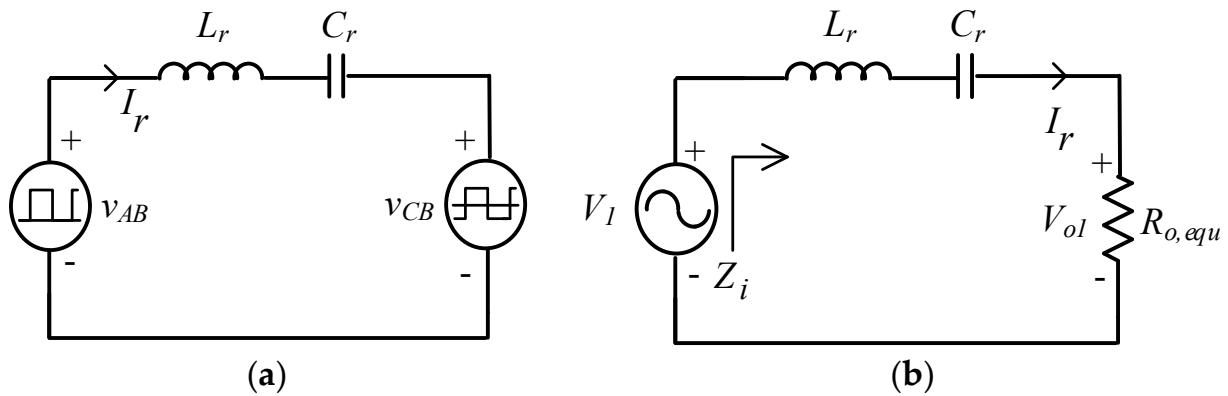
Figure 5. Equivalent circuits (**a**) the series resonant converter, (**b**) fundamental approximated analysis.

It can be known from Equations (9) and (14) that v_{CB} is also a square wave expressed as

$$v_{CB}(t) = \begin{cases} 0.5(V_{o1} + V_{o3}), \text{ for } \theta < \omega t \leq \theta + \pi \\ -0.5(V_{o2} + V_{o4}), \text{ for } \theta + \pi < \omega t \leq \theta + 2\pi \end{cases}. \tag{26}$$

In the practical circuit, the number of LEDs in each string is equal, and LEDs of the same type have almost the same voltage, so

$$V_{o1} \approx V_{o2} \approx V_{o3} \approx V_{o4} \approx V_{LED}, \tag{27}$$

where V_{LED} represents the total voltage of each LED sting. Combining Equations (26) and (27), the Fourier expansion for v_{CB} is

$$v_{CB}(t) = \sum_{n=1, 3, 5, \dots} \frac{4V_{LED}}{n\pi} \sin(2n\pi f_s t) \quad n = 1, 3, 5 \dots \tag{28}$$

The root-mean-square value of the fundamental voltage of v_{CB} is given by

$$V_{o1, rms} = \frac{2\sqrt{2}V_{LED}}{\pi}. \tag{29}$$

When a series resonant circuit has a high loaded quality factor, the current in the resonant tank would be approximately sinusoidal, and the series resonant converter can be approximately analyzed by using the fundamental wave method (FWM). The equivalent circuit for FWM analysis is shown in Figure 5b, where $R_{o,equ}$ is the equivalent load resistance [21,22].

$$R_{o,equ} = \frac{V_{o1,rms}}{I_{r,rms}}. \tag{30}$$

The load quality factor of a series resonant circuit is defined as

$$Q_L = \frac{\sqrt{L_r/C_r}}{R_{o,equ}}. \tag{31}$$

The LED current is supplied from the resonant current. At steady-state operation, the following equation must be satisfied.

$$\frac{2}{T_s} \int_0^{\frac{T_s}{2}} \sqrt{2}I_{r,rms} \sin(2\pi f_s t)dt = 4I_{LED}. \tag{32}$$

The following equation is obtained by solving Equation (32),

$$I_{r,rms} = \sqrt{2}\pi I_{LED}, \tag{33}$$

where I_{LED} represents the current in each LED string. The phasor relationship between V_{o1} and V_1 can be expressed as follows:

$$\vec{V_1} = V_{o1}\angle 0^\circ + jX_s I_r \angle 0^\circ, \tag{34}$$

where the impedance of the resonant tank is

$$X_s = 2\pi f_s L_r - \frac{1}{2\pi f_s C_r}. \tag{35}$$

Using Equation (34), the following equation is derived:

$$(V_{1,rms})^2 = (I_{r,rms} X_s)^2 + (V_{o1,rms})^2. \tag{36}$$

Referring to Figure 2a,b, the following equations can be obtained.

$$v_{CB}(t) = \begin{cases} V_{pri} + 0.7 + V_{o1} = -V_{sec} + 0.7 + V_{o3} & \text{when } D_{o1} \text{and } D_{o3} \text{ are on.} \\ V_{pri} - 0.7 - V_{o2} = -V_{sec} - 0.7 - V_{o4} & \text{when } D_{o2} \text{ and } D_{o4} \text{ are on.} \end{cases} \tag{37}$$

From Equation (37), the primary voltage of T_2 can be expressed as

$$V_{pri}(t) = V_{sec}(t) = \begin{cases} 0.5(V_{o3} - V_{o1}) & \text{when } D_{o1} \text{and } D_{o3} \text{ are on.} \\ 0.5(V_{o2} - V_{o4}) & \text{when } D_{o2} \text{ and } D_{o4} \text{ are on.} \end{cases} \tag{38}$$

4. Circuit Design and Experimental Results

A 72-W LED driver was used as an illustrative example. The circuit specification is listed in Table 1. The load was four LED strings. Each string was composed of six 3-W LEDs. The rated current and rated voltage of each LED were 0.78A and 3.85 V, respectively. The duty ratio and switching frequency of S_1 are 0.45 and 50 kHz, respectively.

Table 1. Circuit specification.

V_{in}	110 V $\pm$ 10% (rms), 60 Hz
P_{LED}	72 W (24 $\times$ 3 W)
V_{LED}	23.1 V (6 $\times$ 3.85 V)
I_{LED}	0.78 A
f_s	50 kHz
D	0.45

4.1. Parameters Design

4.1.1. Parameters of the Flyback Converter

According to Inequality (22), the dc-link voltage is inverse proportion to the turns ratio of T_1. The higher the turns ratio, the lower the dc-link voltage. In this illustrative example, the turns ratio is chosen as 2:1 and, as a result of the calculation of Inequality (22), V_{dc} must be higher than 70 V.

$$V_{dc} > \frac{0.45 \times 110 \times \sqrt{2} \times 1.1}{2(1 - 0.45)} = 70 \text{ V.}$$

Here, the value of V_{dc} is designed to be 100 V. By using Equation (20), the primary inductance of T_1 is calculated based on an assumption of 90% circuit efficiency.

$$L_1 = \frac{0.9 \times \left(110 \times \sqrt{2}\right)^2 \times 0.45^2}{4 \times 72 \times 50 \times 10^3} = 0.306 \text{ mH}.$$

4.1.2. Parameters of the Resonant Converter

The component parameters are calculated from the following steps.

Step 1 Calculate $I_{r,rms}$.

The root-mean-square value of i_r is calculated by using Equation (33).

$$I_{r,rms} = \sqrt{2}\pi \times 0.78 = 3.46 \text{ A}.$$

Step 2 Calculate $V_{1,rms}$ and $V_{o1,rms}$.

The root-mean-square value of V_1 is calculated by using Equation (25).

$$V_{1,\ rms} = \frac{\sqrt{2} \times 100}{\pi} = 45 \text{ V}.$$

As shown in Figure 1, each LED string is connected in series with a diode, and the conduction voltage of the diode is considered when designing the parameters. Referring to Figure 5b, the root-mean-square value of V_{o1} can be calculated from Equation (29).

$$V_{o1,\ rms} = \frac{2\sqrt{2}(0.7 + 23.1)}{\pi} = 21.4 \text{ V}.$$

Step 3 Calculate $R_{o,equ}$ and X_s.

By using Equations (30) and (36), the equivalent load resistance and impedance of the series resonant circuit are calculated, respectively.

$$R_{o,equ} = \frac{V_{o1,rms}}{I_{r,rms}} = \frac{21.4}{3.46} = 6.18 \ \Omega$$

$$X_s = \frac{\sqrt{\left(V_{1,rms}\right)^2 - \left(V_{o1,rms}\right)^2}}{I_{r,rms}} = \frac{\sqrt{(45)^2 - (21.4)^2}}{3.46} = 11.44 \ \Omega.$$

Step 4 Determine Q_L and Calculate L_r and C_r.

Typically, when Q_L is higher than 2, i_r will approach a sinusoid [27]. Here, Q_L is chosen to be 3. Substituting $Q_L = 3$ and $X_s = 11.44 \ \Omega$ into Equations (31) and (35), respectively, the values of L_r and C_r are calculated.

$$C_r = 232 \text{ nF}, L_r = 0.08 \text{ mH}.$$

In order to use standard capacitance value close to 232 nF, C_r is chosen to be 220 nF, and then L_r is recalculated.

$$C_r = 220 \text{ nF}, L_r = 0.0825 \text{ mH}.$$

4.2. Experimental Results

The control circuitry was composed of a microcontroller (dsPIC33FJ16GS504) and two power MOSFET drivers (TLP250). From Equation (20), the LED power can be controlled by regulating the switching frequency of the active switches. A current sensor (ACS712) was used to sense the current in one of the LED strings and send its output to the microcontroller.

Then, the frequency was adjusted to achieve stable LED current. A prototype circuit with the component parameters, as shown in Table 2, was built and tested.

Table 2. Component parameters.

T_1 turns ratio n	2
DC-link Voltage V_{dc}	100 V
Inductor L_f	0.5 mH
Capacitor C_f	2 μF
T_1 primary inductance L_1	0.306 mH
Capacitances C_{dc}, C_{o1}–C_{o4}	100 μF
Resonant Inductance L_r	0.083 mH
Resonant Capacitance C_r	220 nF
Active switches S_1, S_2,	SPW47N60C3
Diodes D_{r1}~D_{r4}, D_1~D_3, D_{o1}~D_{o4}	MUR460

The experimental results at rated power are shown in Figure 6a–g. Figure 6a shows the primary current (the lower waveform) and the secondary current (the upper waveform) in T_1 measured near the peak input voltage. Since the turn ratio of T_1 is 2, it can be seen that the peak value of the secondary current is twice that of the primary current. In addition, the current waveforms indicate that the flyback converter is operated at DCM, as expected. Figure 6b shows the voltage and current of the input line. Both of them are sinusoidal waveforms. As shown, the input current can follow the waveform of the line voltage and in phase with each other. It ensures a high power factor and low THDi. The measured power factor of 0.989 and THDi of 5.27% validate the excellent functionality of the flyback-typed PFC circuit. The drain-to-source voltage and current of S_1 are shown in Figure 6c. By designing the series resonant converter to present inductive characteristics, the resonant current will lag the input voltage of the resonant converter. Therefore, as soon as S_2 is turned off, the resonant current is converted to flow through the parasitic capacitor of S_1. When the parasitic capacitor is discharged to near zero volts (0.7 V), the resonant current will flow through D_{s1} and then the voltage across S_1 is clamped to almost zero volts and the ZVS operation of S_1 is achieved, resulting in low switching losses. However, the shared active switch S_2 cannot fulfill ZVS operation. The drain-to-source voltage and current of S_2 are shown in Figure 6d. Since D_2 prevents the parasitic capacitance of S_2 from discharging to the resonant circuit, a spike current happens due to the short-circuit discharge of the parasitic capacitance as soon as turning on S_2, leading to higher switching-on losses.

Moreover, both currents of the flyback and Class-D converters flow through the shared active switch (S_2). In practice, there is unavoidable leakage inductance in the coupled inductor of the flyback converter. When S_2 is turned off, the current of the leakage inductance cannot be transferred to the resonant circuit. It will flow to and charge the parasitic capacitor of S_2. Since the parasitic capacitor is usually very small, it will not only be charged to high spike voltage (as shown) but also cause high switching losses. Some lossless and passive snubber circuits have been reported to reduce the spike voltage. The resonant current in the series resonant current is shown in Figure 6e. Since the loaded quality factor is high enough, the resonant current is approximately a sine wave with a zero DC component. Figure 6f,g show the voltages and currents of the four LED strings, respectively. The measure voltages are 22.86 V, 23.18 V, 22.53 V, and 23.08 V while the measured currents are 0.75 A, 0.77 A, 0.76 A, and 0.76 A, respectively. The maximum difference of each string current is about 0.02 A, which should be the value of the magnetizing current of T_2. The measured circuit efficiency is 88.2%. As predicted, the LED currents are almost the same; this proves the current balancing capability.
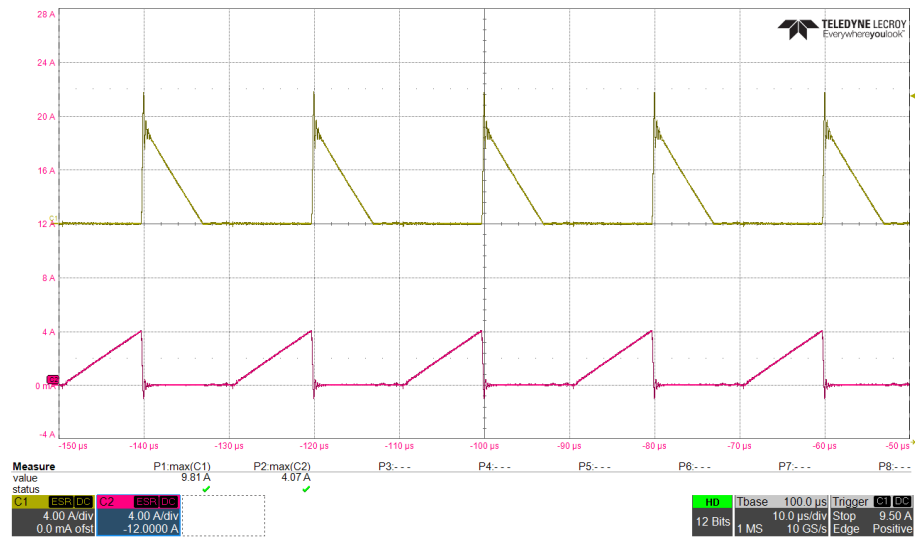
(**a**)
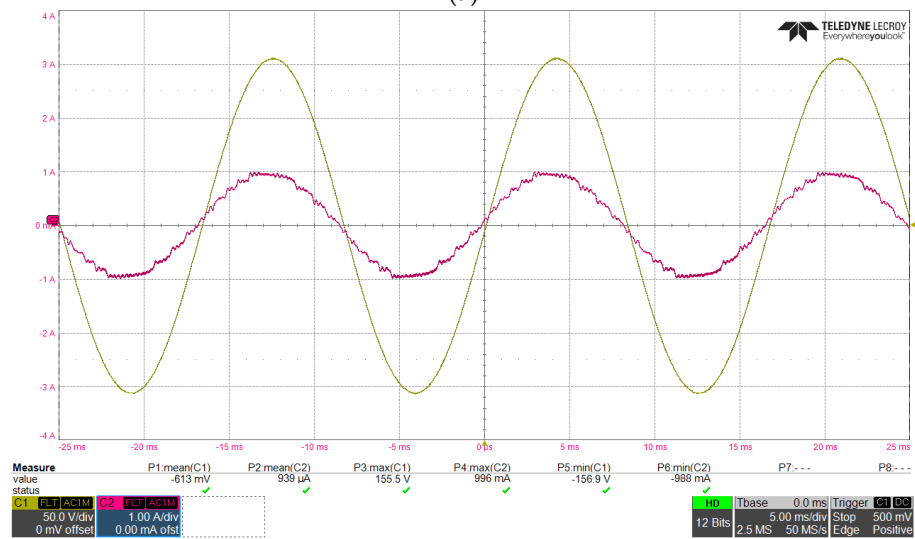
(**b**)
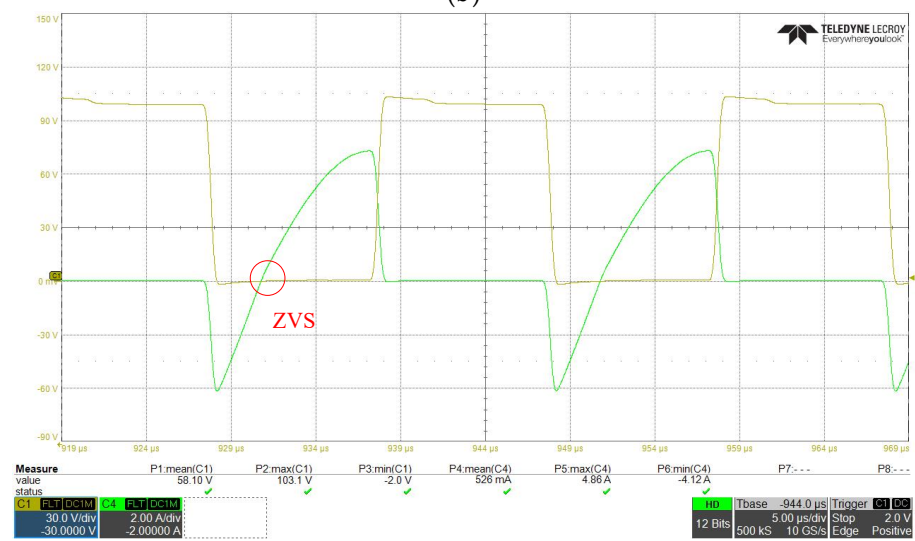
(**c**)

Figure 6. *Cont.*
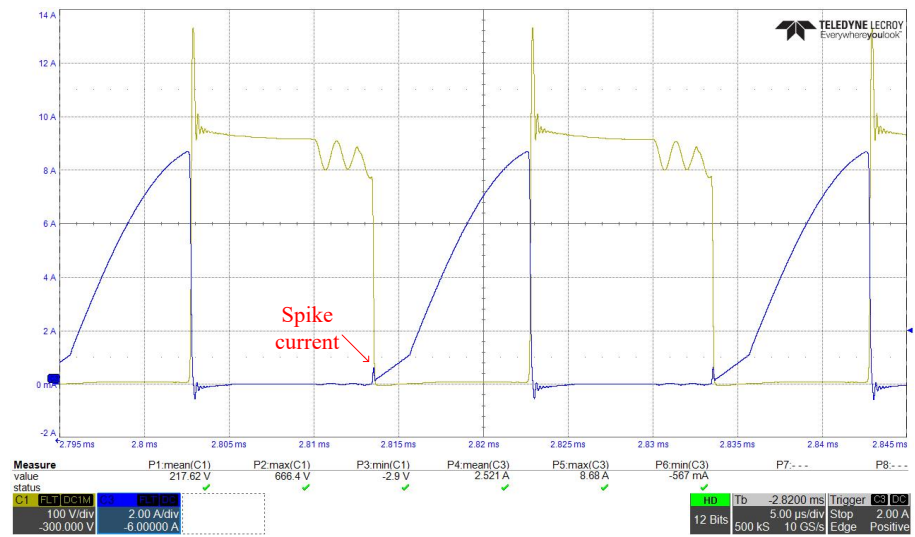
(**d**)
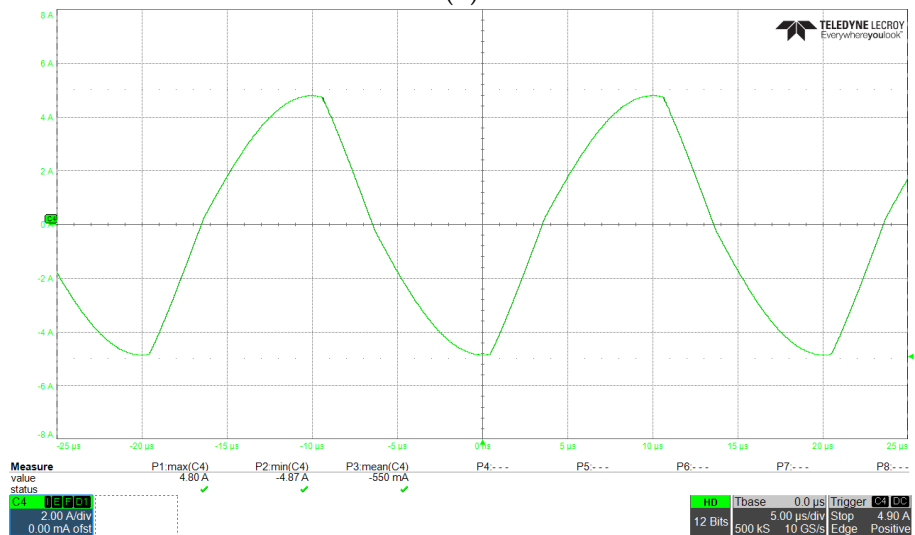
(**e**)
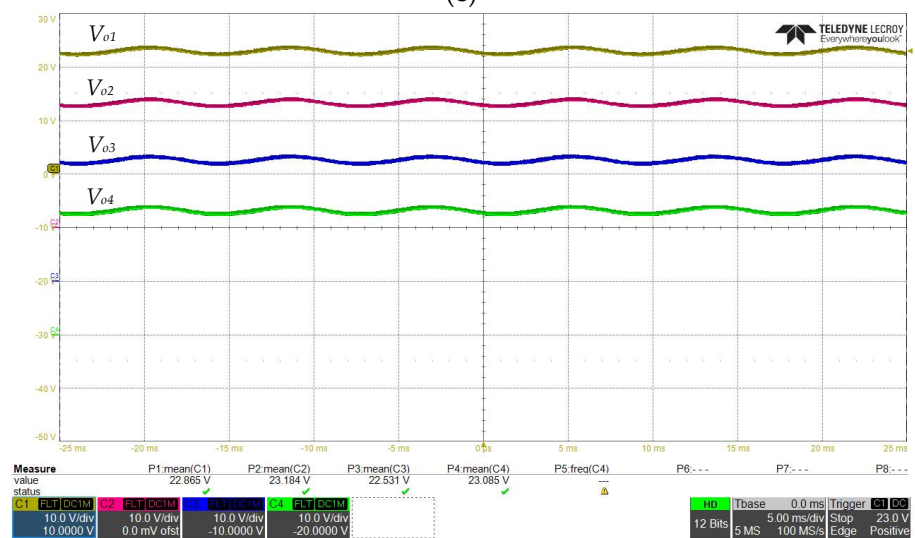
(**f**)

Figure 6. *Cont.*
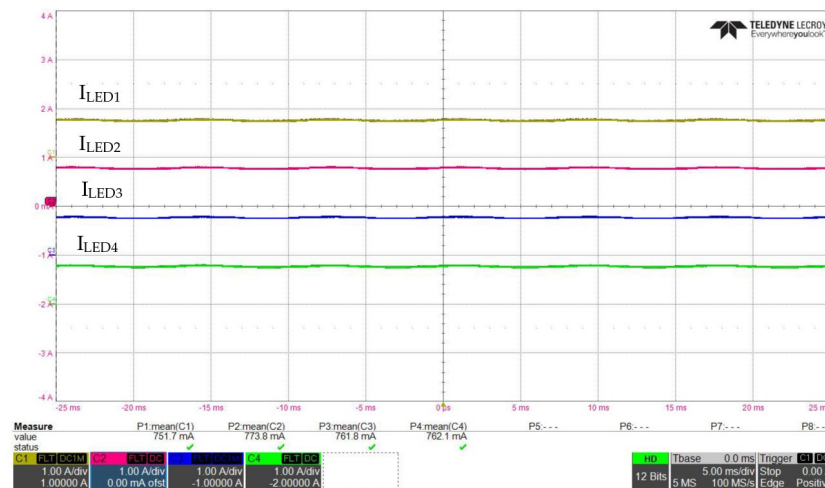
(g)

Figure 6. (**a**) Waveforms of the primary and secondary currents of T_1. (i_{L1}, i_{L2}: 4 A/div, time: 10 μs/div). (**b**) Waveforms of the input voltage and current. (v_{in}: 50 V/div, i_{in}: 1.0 A/div, time: 5 ms/div). (**c**) Voltage and current waveforms of S_1. (v_{DS1}: 30 V/div, i_{S1}: 2.0 A/div, time: 5 μs/div). (**d**) Voltage and current waveforms of S_2. (v_{DS2}: 50 V/div, i_{S2}: 2.0 A/div, time: 5 μs/div). (**e**) Waveforms of the resonant current. (i_r: 2.0 A/div, time: 5 μs/div). (**f**) Waveforms of V_{o1}, V_{o2}, V_{o3} and V_{o4} for the 4 LED strings. (voltages: 10 V/div, time: 5 ms/div). (**g**) Waveforms of I_{LED1}, I_{LED2}, I_{LED3} and I_{LED4} for the 4 LED strings. (currents: 1.0 A/div, time: 5 ms/div).

5. Conclusions

The study presented a novel LED driver. The circuit topology of a single stage was derived by integrating a flyback converter and a Class-D series resonant converter. Both converters share an active switch and the control circuit. A near unity power factor is obtained when the flyback converter is operated at DCM. The series resonant converter combines a differential-mode transformer with a turn ratio of 1. With the function of series resonant circuit and 1:1 transformer, the current of four LED strings can be automatically equalized, without any additional control circuit for current balancing. The measured power factor is as high as 0.99 and the THDi is 5.27% at the rated power operation. In addition, the experimental results verified that the proposed circuit can indeed achieve the LED current balancing function, and the measured circuit efficiency is 88.2%.

Author Contributions: H.-L.C. designed the circuit and wrote the paper; Y.-C.H. performed circuit simulation and built and measured the prototype circuit. All authors have read and agreed to the published version of the manuscript.

Conflicts of Interest: The authors declare no conflict of interest.

References

1. Li, L.; Gao, Y.; Jiang, H.; Mok, P.K.T.; Lau, K.M. An auto-zero-voltage-switching quasi-resonant LED driver with GaN FETs and fully integrated LED shunt protectors. *IEEE J. Solid-State Circuits* **2018**, *53*, 913–923. [CrossRef]
2. Lee, E.S.; Choi, B.H.; Nguyen, D.T.; Jang, G.C.; Rim, C.T. Versatile LED drivers for various electronic ballasts by variable switched capacitor. *IEEE Trans. Power Electron.* **2016**, *31*, 1489–1502. [CrossRef]

3. Esteki, M.; Khajehoddin, S.A.; Safaee, A.; Li, Y. LED system applications and LED driver topologies: A review. *IEEE Access* **2023**, *11*, 38324–38358. [CrossRef]
4. Liu, X.; Zhou, Q.; Xu, J.; Lei, Y.; Wang, P.; Zhu, Y. High-efficiency resonant LED backlight driver with passive current balancing and dimming. *IEEE Trans. Ind. Electron.* **2018**, *65*, 5476–5486. [CrossRef]
5. Zhao, C.; Xie, X.; Liu, S. Multioutput LED drivers with precise passive current balancing. *IEEE Trans. Power Electron.* **2013**, *28*, 1438–1448. [CrossRef]
6. Chiu, H.J.; Cheng, S.J. LED backlight driving system for large-scale LCD panels. *IEEE Trans. Ind. Electron.* **2007**, *54*, 2751–2760. [CrossRef]
7. Li, S.N.; Zhong, W.X.; Chen, W.; Hui, S.Y.R. Novel self-configurable current-mirror techniques for reducing current imbalance in parallel light-emitting diode (LED) strings. *IEEE Trans. Power Electron.* **2012**, *27*, 2153–2162. [CrossRef]
8. Li, S.; Hui, S.Y.R. Self-configurable current-mirror circuit with short-circuit and open-circuit fault tolerance for balancing parallel light-emitting diode (LED) string current. *IEEE Trans. Power Electron.* **2014**, *29*, 5498–5550. [CrossRef]
9. Qu, X.; Wong, S.C.; Tse, C.K. Noncascading structure for electronic ballast design for multiple LED lamps with independent brightness control. *IEEE Trans. Power Electron.* **2010**, *25*, 331–340.
10. Kim, J.W.; Moon, J.P.; Moon, J.W. Duty-ratio-control-aided LLC converter for current balancing of two-channel LED driver. *IEEE Trans. Ind. Electron.* **2017**, *64*, 1178–1184. [CrossRef]
11. Chen, H.; Zhang, Y.; Ma, D. A SIMO parallel-string driver IC for dimmable LED backlighting with local bus voltage optimization and single time-shared regulation loop. *IEEE Trans. Power Electron.* **2012**, *27*, 452–462. [CrossRef]
12. Yang, W.H.; Yang, H.A.; Huang, C.J.; Chen, K.H. A high-efficiency single-inductor multiple-output buck-type LED driver with average current correction technique. *IEEE Trans. Power Electron.* **2018**, *33*, 3375–3385. [CrossRef]
13. Qu, X.; Wong, S.C.; Tse, C.K. An improved LCLC current-source-output multistring LED driver with capacitive current balancing. *IEEE Trans. Power Electron.* **2015**, *30*, 5783–5791. [CrossRef]
14. Wu, X.; Zhang, J.; Qian, Z. Multichannel LED driver with CLL resonant converter. *IEEE Trans. Emerg. Sel. Top. Power Electron.* **2015**, *3*, 589–598.
15. Liu, T.; Liu, X.; He, M.; Zhou, S.; Meng, X.; Zhou, Q. Flicker-free resonant LED driver with high power factor and passive current Balancing. *IEEE Access* **2020**, *9*, 6008–6017. [CrossRef]
16. Jiang, W.Z.; Hwu, K.I.; Chen, H.H. Applying hybrid passive current-sharing components to non-isolated LED driver. In Proceedings of the 2020 International Symposium on Computer, Consumer and Control, Taichung, Taiwan, 13–16 November 2020; pp. 259–262.
17. Ye, Y.; Cheng, K.W.; Lin, J.; Wang, D. Single-switch multichannel current-balancing LED drive circuits based on optimized SC techniques. *IEEE Trans. Ind. Electron.* **2015**, *62*, 4761–4768. [CrossRef]
18. Liu, X.S.; Yang, Q.; Zhou, Q.; Xu, J.P.; Zhou, G.H. Single-stage single-switch four-output resonant LED driver with high power factor and passive current balancing. *IEEE Trans. Power Electron.* **2017**, *32*, 4566–4576. [CrossRef]
19. Gücin, T.N.; Fincan, B.; Biberoğlu, M. A series resonant converter-based Multichannel LED driver with inherent current balancing and dimming capability. *IEEE Trans. Power Electron.* **2019**, *34*, 2693–2703. [CrossRef]
20. Guan, Y.; Cai, H.; Zhang, X.; Wang, Y.; Wang, W.; Xu, D. A soft-switching transformer-less step-down converter based on resonant current balance Module. In Proceedings of the IEEE Industry Applications Society Annual Meeting, Detroit, MI, USA, 11–15 October 2020.
21. Wang, Y.; Guan, Y.; Ren, K.; Wang, W.; Xu, D. A single-stage LED driver based on BCM boost circuit and *LLC* converter for street lighting system. *IEEE Trans. Ind. Electron.* **2015**, *62*, 5446–5457. [CrossRef]
22. Lu, D.D.C.; Iu, H.H.C.; Pjevalica, V. Single-stage ac/dc boost-forward converter with high power factor and regulated bus and output voltages. *IEEE Trans. Ind. Electron.* **2009**, *56*, 2128–2132. [CrossRef]
23. Wang, Y.; Hu, X.; Guan, Y.; Xu, D. A single-stage LED driver based on half-bridge CLCL resonant converter and buck–boost circuit. *IEEE Trans. Power Electron.* **2019**, *7*, 196–208. [CrossRef]
24. Liu, X.; Wan, Y.; Dong, Z.; He, M.; Zhou, Q.; Tse, C.K. Buck–boost–buck-type single-switch multistring resonant LED driver with high power factor and passive current balancing. *IEEE Trans. Power Electron.* **2020**, *35*, 5132–5143. [CrossRef]
25. Cheng, H.L.; Chang, Y.N.; Chang, C.H.; Hsieh, S.Y.; Cheng, C.A. A novel high-power-factor AC/DC LED driver with dual flyback converters. *IEEE Trans. Emerg. Sel. Topics Power Electron.* **2019**, *7*, 555–564. [CrossRef]
26. Hwu, K.I.; Chou, S.C. A simple current-balancing converter for LED lighting. In Proceedings of the Twenty-Fourth Annual IEEE Applied Power Electronics Conference and Exposition, Washington, DC, USA, 15–19 February 2009; pp. 587–590.
27. Kazimierczuk, M.K.; Czarkowski, D. *Resonant Power Converters*, 1st ed.; John Wiley & Sons: New York, NY, USA, 1995; pp. 149–198.